Calcium-dependent dynamics of cadherin interactions at cell–cell junctions

Sally A. Kim[a,1], Chin-Yin Tai[a,1,2], Lee-Peng Mok[a], Eric A. Mosser[a], and Erin M. Schuman[a,b,3]

[a]Division of Biology, California Institute of Technology, Pasadena, CA 91125; and [b]Max Planck Institute for Brain Research, D-60528 Frankfurt am Main, Germany

Edited* by Barry H. Honig, Columbia University/Howard Hughes Medical Institute, New York, NY, and approved May 2, 2011 (received for review December 17, 2010)

Cadherins play a key role in the dynamics of cell–cell contact formation and remodeling of junctions and tissues. Cadherin–cadherin interactions are gated by extracellular Ca^{2+}, which serves to rigidify the cadherin extracellular domains and promote *trans* junctional interactions. Here we describe the direct visualization and quantification of spatiotemporal dynamics of *N*-cadherin interactions across intercellular junctions in living cells using a genetically encodable FRET reporter system. Direct measurements of transjunctional cadherin interactions revealed a sudden, but partial, loss of homophilic interactions ($\tau = 1.17 \pm 0.06\ s^{-1}$) upon chelation of extracellular Ca^{2+}. A cadherin mutant with reduced adhesive activity (W2A) exhibited a faster, more substantial loss of homophilic interactions ($\tau = 0.86 \pm 0.02\ s^{-1}$), suggesting two types of native cadherin interactions—one that is rapidly modulated by changes in extracellular Ca^{2+} and another with relatively stable adhesive activity that is Ca^{2+} independent. The Ca^{2+}-sensitive dynamics of cadherin interactions were transmitted to the cell interior where β-catenin translocated to *N*-cadherin at the junction in both cells. These data indicate that cadherins can rapidly convey dynamic information about the extracellular environment to both cells that comprise a junction.

cell adhesion | fluorescence resonance energy transfer | trans binding

The junctions between cells are populated with a variety of cell adhesion molecules that drive the recognition, assembly, and dynamics of cell–cell interactions. Parsing the distinct functions of different adhesion molecules has been challenging, in part due to a paucity of truly revealing in vivo assays. Among cell adhesion molecule families, the classic cadherins exhibit a unique dependence on extracellular Ca^{2+} to rigidify the extracellular domains and enable *trans* junctional homophilic interactions. Three Ca^{2+} ions bind with different affinities to each of the pockets between cadherin extracellular domains (1, 2). The affinity of the various Ca^{2+} binding sites is in the micromolar to millimolar range (3–8), suggesting the possibility that cadherins can respond dynamically to changes in junctional Ca^{2+} levels, and by virtue of physical interactions with cytoplasmic molecules, signal information about the junctional status to the cell interior.

3D reconstructions of desmosomes by cryoelectron tomography reveal cadherins interact across intercellular interfaces (9, 10), and crystallographic data of several cadherin domains (4, 11, 12) implicate the first two extracellular repeats (ECs 1 and 2) as critical for homophilic interactions. Previous studies have indicated the importance of a highly conserved tryptophan residue (Trp2), present in the first EC domain, for cadherin-dependent adhesion (2, 12). This tryptophan inserts into the hydrophobic pocket of the partner *N*-cadherin (Ncad) molecule to form a strand-swapped dimeric structure (11, 12). Mutation of Trp2 to an alanine residue (W2A) prevents strand swapping (13) and results in a loss of adhesive function (2, 14, 15). Although extensive work has elucidated the structure (4, 9–14), biochemistry (2, 16) and single-molecule characterization (15, 17) of cadherin adhesion, relatively little is known about these interactions and their dynamics in living cells.

In this work we develop a genetically encoded fluorescence reporter system that enables the visualization and quantification of spatiotemporal dynamics of *N*-cadherin interactions across intercellular junctions in live cells. We show that *N*-cadherin molecules exhibit a sudden, partial loss of interaction upon rapid removal of extracellular Ca^{2+}. In comparison, a variant with a point mutation (W2A) that substantially decreases adhesive activity exhibited a faster, more substantial loss with Ca^{2+} chelation, These data reveal a much greater structural change due to Ca^{2+} depletion in the absence of the Trp2-hydrophobic pocket interaction of EC1 and suggest a cadherin–cadherin interaction in the wild-type protein that is Ca^{2+} independent but Trp2 dependent. Furthermore, β-catenin, an intracellular binding partner of *N*-cadherin that mediates the association of cadherins with the actin cytoskeleton, translocates to the junction in both cells upon Ca^{2+} removal. We postulate that the rapid Ca^{2+} sensing property of cadherin molecules may coordinate adhesion and allow for both cells to access information about junctional status simultaneously and signal this information to the cell interior.

Results and Discussion

To examine the spatiotemporal dynamics of cadherin interactions, we designed a genetically encodable intermolecular FRET-based reporter system that exploits the physical interaction of cadherins at junctions and uses Cerulean fluorescent protein (FP) as the FRET donor (18) and Venus FP as the FRET acceptor (19) (Fig. 1*A*). The dimensions of each cadherin EC are known to be ~45 Å long × 25 Å diameter. Based on this, we hypothesized that Cerulean and Venus (~42 Å in length × 24 Å diameter barrel) (20) inserted within the first two distal EC domains would be within the calculated Förster distance (R_0 = 54 Å for Cerulean and Venus) (21) and efficiently report cadherin interactions across junctions (Fig. 1*A*).

To insert a GFP into the compact extracellular domain of *N*-cadherin without affecting its function, we performed an in vitro transposition screen to isolate functional clones (22). We screened 509 colonies and found four clones that had GFP inserted in the distal extracellular region (from the N terminus of the first EC to the C terminus of the second EC). From this screen, we chose a clone with GFP inserted in one of the solvent-exposed helices in extracellular domain 2 (FP-Ncad; Fig. 1*B*) (2) that had the brightest expression at cell–cell contacts. We

Author contributions: S.A.K., C.-Y.T., L.-P.M., E.A.M., and E.M.S. designed research; S.A.K., C.-Y.T., and L.-P.M. performed research; S.A.K., C.-Y.T., and L.-P.M. contributed new reagents/analytic tools; S.A.K., C.Y.T., and L.-P.M. analyzed data; and S.A.K. and E.M.S. wrote the paper.

The authors declare no conflict of interest.

*This Direct Submission article had a prearranged editor.

[1]S.A.K. and C.-Y.T. contributed equally to this work.

[2]Present address: Institute of Molecular Biology, Academica Sinica, Nankang, Taipei 115, Taiwan, Republic of China.

[3]To whom correspondence should be addressed. E-mail: schumane@brain.mpg.de.

This article contains supporting information online at www.pnas.org/lookup/suppl/doi:10.1073/pnas.1019003108/-/DCSupplemental.

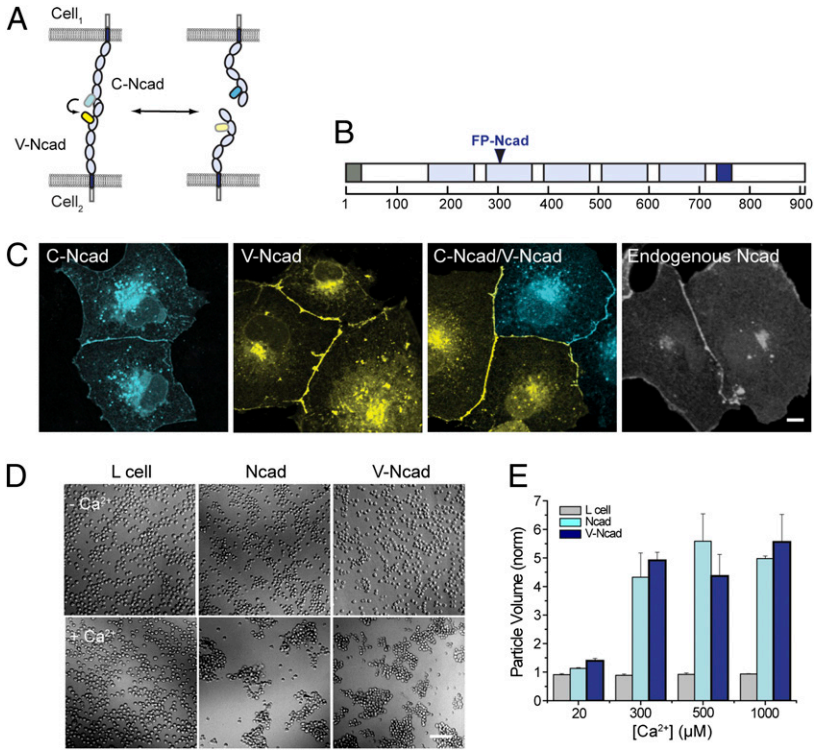

Fig. 1. Design and characterization of *N*-cadherin FRET reporter. (*A*) Schematic of *N*-cadherin–*N*-cadherin interactions at cell–cell junctions monitored by FRET. Light blue ovals represent the five EC domains; the inserted fluorescent protein, Venus (yellow) or Cerulean (cyan), is located in the EC2 domain. Dynamic interactions of cadherins monitored by FRET result in intensity changes of each fluorescent protein. (*B*) Domain structure of fluorescent protein insertion site in *N*-cadherin (gray, signal peptide; light blue, EC domains; dark blue, transmembrane domain; blue arrow, FP insertion site). Amino acid numbers are indicated below the bar. (*C*) *N*-cadherin fusion proteins. Cerulean (*Left*), Venus (*Center Left*), and Cerulean/Venus (*Center Right*) localize to the membrane and form cell–cell contacts similar to the localization of endogenous Ncad (*Right*) in COS-7 cells. (Scale bar: 10 μm.) (*D*) L-cells expressing Ncad or V-Ncad constructs show robust cell aggregation under high Ca^{2+} (1 mM Ca^{2+}). (Scale bar: 50 μm.) (*E*) Ncad and V-Ncad stable cell lines show similar and increasing aggregation with increasing extracellular Ca^{2+} concentrations. No statistically significant differences (Student *t* test; $P < 0.05$) were seen at higher Ca^{2+} concentrations (300–1,000 μM). Error bars indicate ± SEM for $n = 3$–4 for each condition. Untransfected L-cells showed no aggregation under any conditions.

replaced the GFP with Cerulean or Venus and then transfected two separate populations of COS-7 cells with either Cerulean (C-Ncad) or Venus cadherin (V-Ncad). Later, individual populations or mixed populations were plated to examine the junctional localization. Junctions comprising either a single cadherin-fluorescent species (C-Ncad or V-Ncad) or mixed junctions (C-Ncad and V-Ncad) exhibited the appropriate membrane localization of cadherin molecules at cell–cell interfaces, similar to endogenous cadherin (Fig. 1*C*).

We next examined whether our fluorescently labeled cadherin fusion proteins retained Ca^{2+}-dependent adhesion with similar Ca^{2+} binding properties to wild-type cadherin. L-cells that lack endogenous cadherins have been used extensively for cadherin-dependent adhesion function assays (23, 24). In L-cells stably transfected with either unlabeled wild-type Ncad or V-Ncad, comparable levels of total cadherin were expressed in each cell line with the majority of expression on the cell surface (Figs. S1 and S2). We assessed Ca^{2+}-dependent cell aggregation of these stable lines using a quantitative short-term aggregation assay. V-Ncad conferred Ca^{2+}-dependent adhesion to L cells similar to wild-type Ncad within a physiologically relevant Ca^{2+} concentration range (Fig. 1 *D* and *E* and Fig. S3). In contrast, the untransfected L-cells showed no detectable aggregation under any conditions, as expected. Furthermore, fluorescently labeled cadherin fusion proteins interacted with their intracellular binding protein, β-catenin, as detected by immunoprecipitation and immunoblotting (Fig. S4). These results indicate that the fluorescent *N*-cadherin protein fusions exhibit features similar to endogenous *N*-cadherins, including membrane localization, Ca^{2+}-dependent adhesion, and interaction with β-catenin.

To assess the molecular interaction of cadherins under basal conditions in living cells, we performed acceptor bleach FRET experiments on junctions of adjacent transfected COS-7 cells expressing either V-Ncad or C-Ncad fusion proteins (Fig. 2*A*). Following acceptor bleaching of V-Ncad at well-defined two-color junctions, donor dequenching of C-Ncad was observed (Fig. 2*A*), indicating that the fluorescent molecules from the two different cell membranes were well within the distance required for FRET. The average FRET efficiency (34.1 ± 2.32%; mean ± SEM; $n = 10$; Fig. 2*E*) for the wild-type Ncad interactions in living cells most likely represents the molecules in a strand-swapped *trans* dimer configuration (13). Because FRET is distance dependent, we examined the spatial limits for transjunctional FRET using a different clone with an insertion site between EC5 and the transmembrane domain found in our transposition screen (Fig. 2*F*, red arrow, referred to as FP_{prox}-Ncad). Although FP_{prox}-Ncad localized to cell–cell contacts (Fig. 2*B*), the average FRET efficiency was markedly less than FP-Ncad (6.6 ± 1.01%; mean ± SEM; $n = 10$; Fig. 2*E*), as expected from the relatively remote positions of the fluorophores (Fig. 2*F*). As a control, measurements in well-defined single-color junctions of cells expressing V-Ncad or C-Ncad alone indicated no evidence of photoconversion of Venus into a Cerulean-like species as previously reported (25). In additional analyses we were able to quantify and qualitatively map the Ncad interactions assessed by FRET within live cellular contacts, revealing an apparent spatial heterogeneity of Ncad binding within junctions with small

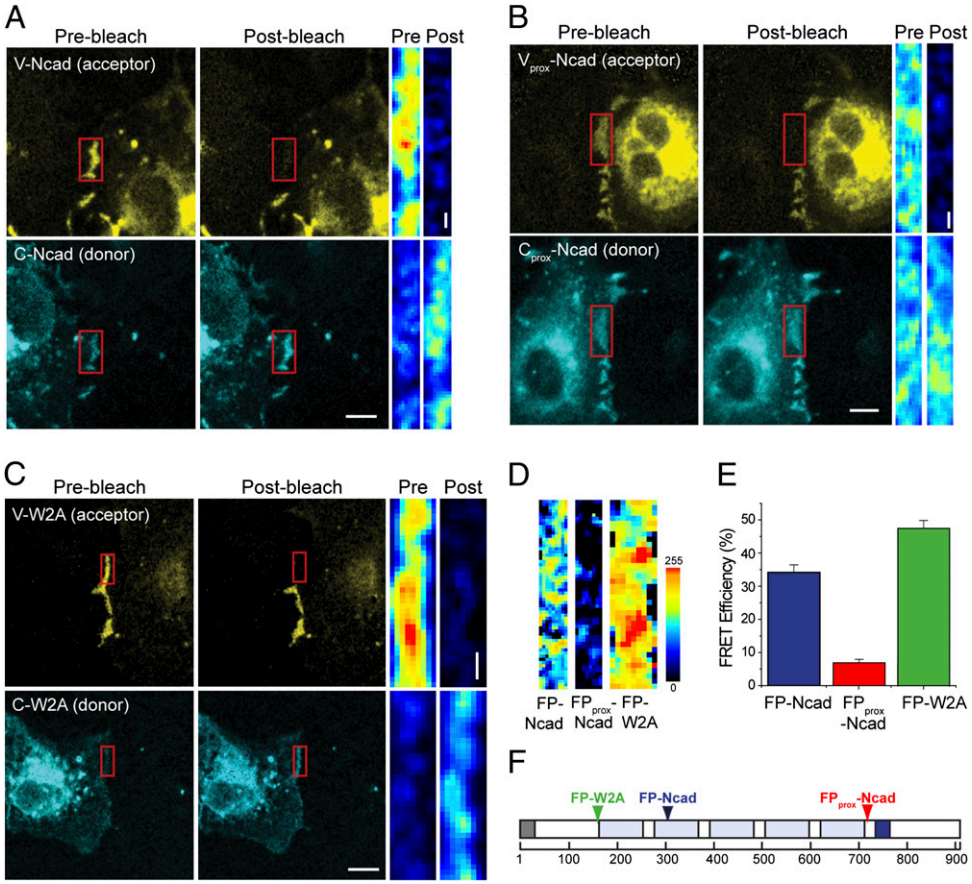

Fig. 2. Detecting *N*-cadherin interactions under basal conditions across cell–cell junctions. A representative example of a cell–cell junction of two adjacent transfected COS-7 cells expressing (*A*) V-Ncad or C-Ncad, (*B*) V_{prox}-Ncad or C_{prox}-Ncad, and (*C*) V-W2A or C-W2A fusion proteins under basal high Ca^{2+} conditions (1.8 mM Ca^{2+}). The acceptor (Venus fusion protein) was bleached within the ROI (red box); images were acquired before and after bleaching (see *D* for color look-up table). (Scale bars: images, 10 μm; corresponding ROIs, 1 μm.) (*D*) Quantitative spatial FRET maps for each of the examples shown in *A*–*C*, respectively, show the heterogeneity of cadherin interactions at cell–cell contact. (Scale bar: same as for corresponding ROIs in *C*.) (*E*) Average FRET efficiencies for WT, W2A, and WT_{prox} *N*-cadherin junctions. Error bars indicate ± SEM for $n = 10$ cells each. (*F*) *N*-cadherin domain structure indicating the W2A mutation (green; FP-W2A), and distal (blue; FP-Ncad) and proximal (red; FP_{prox}-Ncad) insertion sites for FRET reporter constructs.

(<1–2 μm) regions showing much stronger FRET than adjacent areas (Fig. 2*D*).

An important amino acid responsible for cadherin–cadherin adhesion is the highly conserved Trp2, present in the first EC domain, which inserts into the hydrophobic pocket of the partner *N*-cadherin molecule (2, 3, 12). Mutation of Trp2 to an alanine residue (W2A) prevents strand-swapping and results in substantially reduced cadherin homophilic interactions (2, 3). Similar to *N*-cadherin (FP-Ncad) expression in L cells, FP-W2A exhibited membrane localization but with less of the total cellular surface area comprising contacts with neighboring cells (Figs. S1 and S2). The V-W2A cell line exhibited modest aggregation but only at higher Ca^{2+} concentrations (Student *t* test; $P < 0.05$; Figs. S3 and S5), reflecting a markedly weaker binding and confirming similar previous findings (13, 15). Expression of FP-W2A in COS-7 cells, which also possess endogenous cadherins, allowed us to assess the nature of the relationship of FP-W2A cadherins at intact junctions. Although reduced adhesion was observed in L-cells expressing FP-W2A, FP-W2A cadherin mutants exhibited a higher average FRET efficiency (47.3 ± 2.30%; mean ± SEM, $n = 10$; Fig. 2*E*) compared with FP-Ncad (Student *t* test; $P < 0.001$), indicating that the W2A molecules are closer together than wild-type NCad. These data are consistent with recent structural data comparing wild-type and W2A dimeric configurations, in which the wild-type *trans* dimer in a strand-swapped configuration was found to have a markedly wider angle between paired EC1-2 domains compared with the W2A mutant (13). Due to the placement of our label within the EC2 domain, our FRET measurements directly demonstrate these structural differences in living cell–cell junctions (Fig. 2*F*).

Electron microscopic observations of purified E-cadherin EC domains indicate a progressive rigidification of the modular rod-like structure as the Ca^{2+} concentration is increased from <50 μM to >1 mM (4). In vivo, the average basal extracellular Ca^{2+} concentration is 1.5–2 mM (26), well within the range where cadherins engage in *trans* interactions. To test directly whether a change in extracellular Ca^{2+} can be detected by cadherins, we continuously monitored FRET at two-color *N*-cadherin (FP-NCad) junctions in live cells before and after the chelation of extracellular Ca^{2+} (via the addition of EGTA; Fig. 3 *A* and *B*, *Upper*). The rapid addition of EGTA allowed us to evaluate dynamic changes in the molecular geometry of the labeled cadherins and couple the consequences to signaling. Addition of EGTA triggered a rapid and substantial loss of FRET efficiency (Fig. 3*D* and Fig. S6), resulting from simultaneous and reciprocal changes in C-Ncad and V-Ncad fluorescence intensities. Emission spectra before and after Ca^{2+} chelator addition indicated a decrease in the Venus emission signal near 530 nm and a corresponding increase in the Cerulean emission signal near 497 nm (Fig. 3*C*). In control measurements, single-color junctions showed

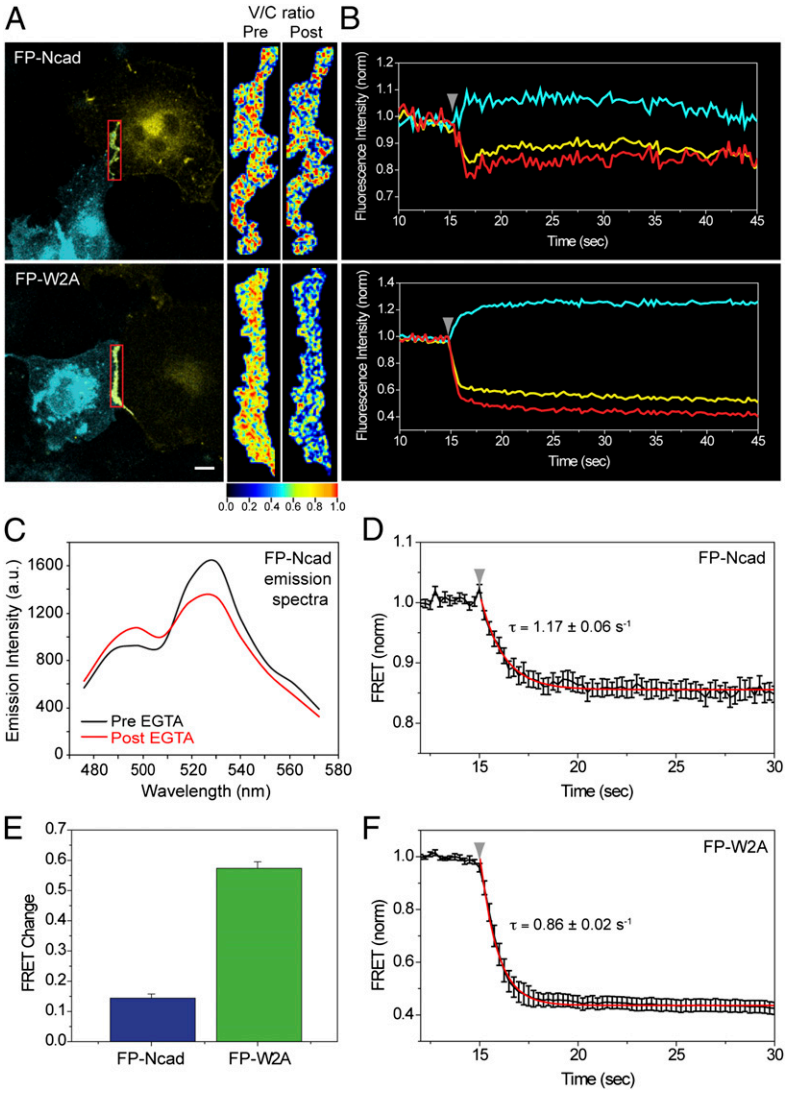

Fig. 3. *N*-cadherin interactions across junctions exhibit a rapid sensitivity to extracellular Ca^{2+} changes. (*A*) Images of COS-7 cells expressing either FP-Ncad or FP-W2A fluorescent fusion proteins of the FRET reporter. ROIs (red boxes) were chosen encompassing well-defined junctions for faster acquisition. ROIs were colorized according to the emission ratio of V-Ncad: C-Ncad fluorescence intensity (V/C ratio). (Scale bar: 10 μm.) (*B*) Quantitation of Ca^{2+}-dependent cadherin FRET changes over time. ROIs (red boxes in *A*) at two-color junctions were imaged before and after the addition of the Ca^{2+} chelator, EGTA (20 mM final), at 15 s (gray arrow). The fluorescence intensity of each channel was normalized to the average baseline (yellow for V-Ncad and cyan for C-Ncad) and plotted together with the V/C ratio as a measure of FRET (red). (*C*) Representative emission spectra of a two-color FP-Ncad junction before and after EGTA treatment. (*D* and *F*) Kinetics of the FRET decrease upon Ca^{2+} removal. EGTA was added at 15 s (see gray arrow; FP-Ncad (*D*) and FP-W2A (*F*); n = 17 each; mean ± SEM). Data were fit with a single exponential decay curve (red). (*E*) Summary of the magnitude of FRET changes upon Ca^{2+} depletion in FP-Ncad and FP-W2A junctions (n = 17 each; $P < 0.0001$).

no significant changes in fluorescence intensity upon extracellular Ca^{2+} chelation (Fig. S7). The reduction in cadherin–cadherin interaction at these junctions exhibited kinetics that was well fit by a single exponential (τ =1.17 ± 0.06 s^{-1}, mean ± SEM; n = 17; Fig. 3*D*). In the continued presence of EGTA, the FRET loss at FP-Ncad junctions reached steady-state and remained stable for the duration of the experiment (Fig. 3 and Fig. S6). Another Ca^{2+} chelator, BAPTA, also elicited similar results.

Given the residual cadherin–cadherin interaction that appeared Ca^{2+} insensitive in the above experiment, we considered the possibility that the molecularly distinct adhesive interface conferred by the Trp2 residue might provide structural stability that maintains some cadherin proximity in the absence of Ca^{2+}. To address this, we examined the behavior of the FP-W2A cadherin mutants following a rapid reduction in Ca^{2+}. Upon chelation of Ca^{2+}, FP-W2A junctions exhibited significantly faster kinetics (τ = 0.86 ± 0.02 s^{-1}; mean ± SEM; n = 17; Fig. 3*F* and Fig. S8) and a substantially greater decrease in FRET compared with FP-Ncad junctions (FRET change for FP-Ncad: 14.43 ± 1.33%, FP-W2A: 57.36 ± 2.13%; n = 17 each; $P <$ 0.0001; Fig. 3*E*). The estimated change in intermolecular distance between FP-W2A before and after the addition of EGTA was much larger than for the FP-NCad.

Taken together, our data reveal a much greater structural change due to Ca^{2+} depletion in the absence of the Trp2-hydrophobic pocket interaction of EC1 and indicate a cadherin–cadherin interaction in the wild-type molecule that is Ca^{2+} independent. These findings may represent (*i*) a mixed population of dynamic molecules, some which unbind, similar to the W2A dimer configuration, and others that exhibit stable, EGTA-resistant interactions (represented by the remaining residual FRET efficiency); (*ii*) a population that converts to a different stable state (following EGTA treatment) where the fluorophores move to a less favorable FRET orientation; or (*iii*) a combination of all of the above. The current data does not allow us to determine which of these interpretations is correct, but future research will provide more insight into these different states of wild-type *N*-cadherin interactions upon unbinding.

The homophilic nature of cadherin associations allows, in principle, for the transmission of information to the interior of both cells that comprise a junction. To monitor whether a change in signaling can be invoked by extracellular Ca^{2+} dynamics and the loss of cadherin interactions, we examined the dynamics of β-catenin, an intracellular binding partner of *N*-cadherin that regulates the interaction of cadherins with the actin cytoskeleton (27). COS-7 cells were transfected with a β-catenin–GFP construct, and two neighboring cells were imaged before and after

chelation of extracellular Ca^{2+}. Upon addition of EGTA, a bidirectional translocation of β-catenin–GFP to cell–cell contacts was observed (immediate onset upon treatment; $\tau = 4.38 \pm 0.25$ s; mean ± SEM; $n = 7$; Fig. 4 *A* and *D*). This increase in β-catenin–GFP fluorescence at the junction was associated with a concomitant decrease in cytosolic fluorescence in both cells during Ca^{2+} removal (Fig. 4*C*). When the same experiment was performed in L-cells that lack endogenous cadherins, β-catenin failed to translocate to the junction (Fig. 4*B*), indicating that the junctional translocation is cadherin dependent. The fast membrane translocation of β-catenin upon Ca^{2+} chelation indicates that information about the extracellular milieu can be rapidly transmitted to the cytoplasm. The recruitment of β-catenin to the junctional membrane likely represents a compensatory mechanism to stabilize cadherin interactions affected by Ca^{2+} chelation. It has been shown previously that catenins can directly influence the adhesive state of cadherins (28).

Our results show that cadherin molecules localized at junctions in living cells adopt structurally distinct conformations and can sense changes in extracellular Ca^{2+} on a rapid timescale. The FRET measured via fluorophores associated with EC2 provides evidence in living cells for recently described cadherin–cadherin structural interactions comparing wild-type and W2A dimeric configurations (13, 15). The W2A mutant described as the "initial encounter complex" (13) or "X-dimer" (17) has been proposed to be an important intermediate step in the assembly and disassembly of strand-swapped dimers. A recently published paper suggests that the X-dimer may not be an essential step in cadherin assembly at cell–cell contacts but instead is likely a critical transition stage for the release of cadherins from junctions (29). In our experiments we found that the W2A mutant was able to form weak adhesive complexes and possessed rapid dissociation kinetics, consistent with it being an intermediate step in disassembly of strand-swapped dimers.

Furthermore, we show that underlying a dynamic Ca^{2+}-dependent change is a residual, EGTA-insensitive component to the wild-type cadherin–cadherin interactions found at cell junctions. The dissociation rate of strand-swapped dimers at cell–cell contacts in vivo may be slower than dissociation kinetics measured in vitro because in vivo dimers are likely reinforced by *cis* interactions (30, 31). A similar Ca^{2+}-independent stability has been described using cross-linking techniques for lateral dimers (32, 33). Previous work examining cadherin dynamics (34) and the Ca^{2+} dependence of cadherin interactions (35) demonstrated changes with a much longer latency (minutes or hours, rather than seconds) than we have observed here. Our data indicate that extracellular Ca^{2+} fluctuations result in a rapid regulation of cadherin interactions, and that these dynamics can invoke changes in intracellular signaling.

The presence of Ca^{2+}-permeable channels and pumps, as well as a large extra/intracellular Ca^{2+} concentration gradient, suggests that the extracellular ionic environment is dynamic. Indeed, extracellular Ca^{2+} fluctuations have been documented in bone (36), cardiac muscle (37), and neuronal synapses (38, 39). Of particular interest is the neuronal synapse where fluctuations of extracellular Ca^{2+} have been described and characterized. Simulations of active synaptic clefts (26, 40) predict that during synaptic activity, Ca^{2+} concentrations in the cleft drop into the range where local synaptic and/or perisynaptic cadherins would lose transinteractions (~0.8–1 mM). In addition, experimental measurements in the synaptic cleft during high-frequency stimulation have shown that Ca^{2+} concentration may drop to as low as 0.3–0.8 mM (41, 42), and Ca^{2+}-dependent inhibition of cadherin function has been observed during synaptic plasticity (43). Biophysical measurements of purified cadherin extracellular domains, using laser tweezers, showed that an extracellular drop in Ca^{2+} from 1.5 to 0.8 mM is predicted to decrease binding of *N*-cadherin by ~40%, whereas a further drop to 0.3 mM would result in a reduction of binding by 85% (44). Thus, the Ca^{2+} dependence of cadherin interactions seems to be appropriately tuned to monitor physiological fluctuations of Ca^{2+} concentrations. The rapid Ca^{2+} sensing property of cadherin molecules

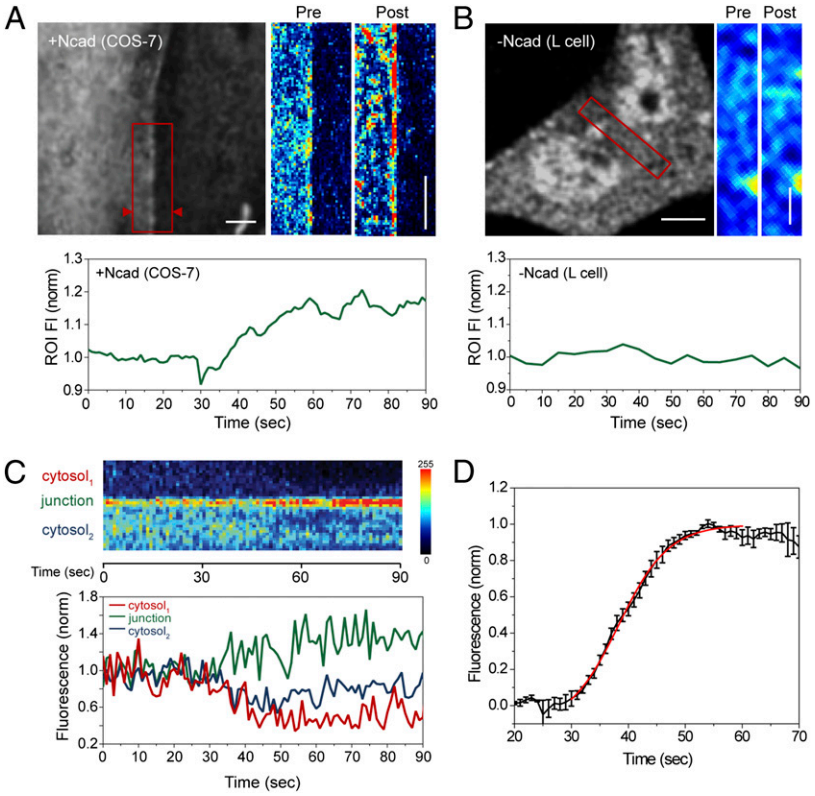

Fig. 4. Extracellular Ca^{2+} chelation results in a translocation of β-catenin to the membrane. β-catenin-GFP is expressed in two neighboring cells in either COS-7 cells with endogenous *N*-cadherin (*A*) or in L-cells in the absence of *N*-cadherin (*B*). Cells were imaged every 1 s before and after the addition of the Ca^{2+} chelator EGTA at 30 s (*A* and *B Upper*). An ROI (red box) of the junctions (*A* and *B Right*) shows pre- and post-EGTA treatment and is pseudocolored according to fluorescence intensity (see *C* for color look-up table). (Scale bars: images, 5 μm; corresponding ROIs, 2 μm.) β-catenin–GFP fluorescence intensity changes in the ROIs were normalized to baseline and plotted over time (*A* and *B Lower*). (*C*) Kymograph showing β-catenin–GFP fluctuations at the junction and neighboring cytosol over time. The one-pixel line scan (marked by the two red arrowheads in *A*) was colorized, and the summary graph indicated a corresponding drop in the cytosol near the junction. (*D*) Kinetics of the β-catenin–GFP fluorescence change upon Ca^{2+} removal. EGTA was added at 30 s ($n = 7$; mean ± SEM). Data were fit with a Boltzmann function (red).

that we document here may coordinate adhesion and signaling across cell–cell junctions, allowing both cells that comprise a junction access to the same information at the same time.

Materials and Methods

FRET Constructs. To generate a functional *N*-cadherin fusion protein with GFP, we used the bacterial transposon-mediated random insertion technique (22) (*SI Materials and Methods*). From our screen, we chose one particular clone with GFP inserted in the extracellular domain (EC2) of cadherin because of its close proximity to the adhesion site at the tip as well as a brighter expression on the membrane and at cell–cell junctions in HEK293 cells. For FRET measurements, the GFP was replaced by Venus and Cerulean. Methods for immunoprecipitation and immunofluorescence have been described previously (45) (*SI Materials and Methods*).

FRET Imaging. Spectral imaging (12-bit, 512 × 512) was accomplished using a LSM510 Meta confocal laser scanning microscope with a 40× 1.3 N.A. oil immersion plan apochromat objective lens (Carl Zeiss MicroImaging, Inc.). A 458-nm argon ion laser was used for excitation. Emitted light was collected over a spectrum of wavelengths between 463 and 580 nm with band widths of 10.7 nm (21). Acceptor bleach FRET was performed by continuous bleaching with the 514-nm laser (100% power, 2,000 iterations) within a chosen ROI. To resolve faster kinetics for time-lapse ratiometric FRET measurements, continuous fast scans (100 ms) of smaller fields of view were used to monitor FRET changes. Because of the significant overlap in the emission spectra of Cerulean and Venus, the fluorescence contribution of each fluorophore at each pixel was separated using a linear unmixing algorithm based on the spectral signatures of Cerulean and Venus created from reference lambda stack images of single-color cell junctions on the same day (21). The mean fluorescence intensity was measured for each fluorophore, and the FRET efficiency was expressed as the emission ratio of Venus:Cerulean. Full methods are provided in *SI Materials and Methods*.

ACKNOWLEDGMENTS. We thank Anh Pham for assistance and the Benson and Piston laboratories for providing the pCXN2-Ncad and mCerulean constructs. We also thank members of the Schuman laboratory, particularly Hwan-Ching Tai and Young Yoon, for helpful discussions, and David Sprinzak, Michael Sutton, Stephanie Bunse, Kaushiki Menon, and especially Kai Zinn, for critical comments on the manuscript. This work was funded by the National Institutes of Health and the Howard Hughes Medical Institute (E.M.S.). S.A.K. was a Damon Runyon Fellow supported by Damon Runyon Cancer Research Foundation Grant DRG-1908-06.

1. Nagar B, Overduin M, Ikura M, Rini JM (1996) Structural basis of calcium-induced E-cadherin rigidification and dimerization. *Nature* 380:360–364.
2. Tamura K, Shan WS, Hendrickson WA, Colman DR, Shapiro L (1998) Structure-function analysis of cell adhesion by neural (N-) cadherin. *Neuron* 20:1153–1163.
3. Chitaev NA, Troyanovsky SM (1998) Adhesive but not lateral E-cadherin complexes require calcium and catenins for their formation. *J Cell Biol* 142:837–846.
4. Pertz O, et al. (1999) A new crystal structure, Ca^{2+} dependence and mutational analysis reveal molecular details of E-cadherin homoassociation. *EMBO J* 18:1738–1747.
5. Koch AW, Pokutta S, Lustig A, Engel J (1997) Calcium binding and homoassociation of E-cadherin domains. *Biochemistry* 36:7697–7705.
6. Pokutta S, Herrenknecht K, Kemler R, Engel J (1994) Conformational changes of the recombinant extracellular domain of E-cadherin upon calcium binding. *Eur J Biochem* 223:1019–1026.
7. Alattia JR, et al. (1997) Lateral self-assembly of E-cadherin directed by cooperative calcium binding. *FEBS Lett* 417:405–408.
8. Prasad A, Pedigo S (2005) Calcium-dependent stability studies of domains 1 and 2 of epithelial cadherin. *Biochemistry* 44:13692–13701.
9. Al-Amoudi A, Díez DC, Betts MJ, Frangakis AS (2007) The molecular architecture of cadherins in native epidermal desmosomes. *Nature* 450:832–837.
10. He W, Cowin P, Stokes DL (2003) Untangling desmosomal knots with electron tomography. *Science* 302:109–113.
11. Boggon TJ, et al. (2002) C-cadherin ectodomain structure and implications for cell adhesion mechanisms. *Science* 296:1308–1313.
12. Shapiro L, et al. (1995) Structural basis of cell–cell adhesion by cadherins. *Nature* 374: 327–337.
13. Harrison OJ, et al. (2010) Two-step adhesive binding by classical cadherins. *Nat Struct Mol Biol* 17:348–357.
14. Overduin M, et al. (1995) Solution structure of the epithelial cadherin domain responsible for selective cell adhesion. *Science* 267:386–389.
15. Sivasankar S, Zhang Y, Nelson WJ, Chu S (2009) Characterizing the initial encounter complex in cadherin adhesion. *Structure* 17:1075–1081.
16. Kitagawa M, et al. (2000) Mutation analysis of cadherin-4 reveals amino acid residues of EC1 important for the structure and function. *Biochem Biophys Res Commun* 271: 358–363.
17. Zhang Y, Sivasankar S, Nelson WJ, Chu S (2009) Resolving cadherin interactions and binding cooperativity at the single-molecule level. *Proc Natl Acad Sci USA* 106: 109–114.
18. Rizzo MA, Springer GH, Granada B, Piston DW (2004) An improved cyan fluorescent protein variant useful for FRET. *Nat Biotechnol* 22:445–449.
19. Nagai T, et al. (2002) A variant of yellow fluorescent protein with fast and efficient maturation for cell-biological applications. *Nat Biotechnol* 20:87–90.
20. Ormö M, et al. (1996) Crystal structure of the Aequorea victoria green fluorescent protein. *Science* 273:1392–1395.
21. Rizzo MA, Springer G, Segawa K, Zipfel WR, Piston DW (2006) Optimization of pairings and detection conditions for measurement of FRET between cyan and yellow fluorescent proteins. *Microsc Microanal* 12:238–254.
22. Sheridan DL, et al. (2002) A new way to rapidly create functional, fluorescent fusion proteins: Random insertion of GFP with an in vitro transposition reaction. *BMC Neurosci* 3:7.
23. Nagafuchi A, Takeichi M (1989) Transmembrane control of cadherin-mediated cell adhesion: A 94 kDa protein functionally associated with a specific region of the cytoplasmic domain of E-cadherin. *Cell Regul* 1:37–44.
24. Alattia JR, Tong KI, Takeichi M, Ikura M (2002) Cadherins. *Methods Mol Biol* 172: 199–210.
25. Valentin G, et al. (2005) Photoconversion of YFP into a CFP-like species during acceptor photobleaching FRET experiments. *Nat Methods* 2:801.
26. Egelman DM, Montague PR (1999) Calcium dynamics in the extracellular space of mammalian neural tissue. *Biophys J* 76:1856–1867.
27. Drees F, Pokutta S, Yamada S, Nelson WJ, Weis WI (2005) Alpha-catenin is a molecular switch that binds E-cadherin-beta-catenin and regulates actin-filament assembly. *Cell* 123:903–915.
28. Gumbiner BM (2005) Regulation of cadherin-mediated adhesion in morphogenesis. *Nat Rev Mol Cell Biol* 6:622–634.
29. Hong S, Troyanovsky RB, Troyanovsky SM (2011) Cadherin exits the junction by switching its adhesive bond. *J Cell Biol* 192:1073–1083.
30. Harrison OJ, et al. (2011) The extracellular architecture of adherens junctions revealed by crystal structures of type I cadherins. *Structure* 19:244–256.
31. Wu Y, et al. (2010) Cooperativity between trans and cis interactions in cadherin-mediated junction formation. *Proc Natl Acad Sci USA* 107:17592–17597.
32. Troyanovsky RB, Laur O, Troyanovsky SM (2007) Stable and unstable cadherin dimers: Mechanisms of formation and roles in cell adhesion. *Mol Biol Cell* 18:4343–4352.
33. Troyanovsky RB, Sokolov E, Troyanovsky SM (2003) Adhesive and lateral E-cadherin dimers are mediated by the same interface. *Mol Cell Biol* 23:7965–7972.
34. Adams CL, Chen YT, Smith SJ, Nelson WJ (1998) Mechanisms of epithelial cell–cell adhesion and cell compaction revealed by high-resolution tracking of E-cadherin-green fluorescent protein. *J Cell Biol* 142:1105–1119.
35. Rothen-Rutishauser B, Riesen FK, Braun A, Günthert M, Wunderli-Allenspach H (2002) Dynamics of tight and adherens junctions under EGTA treatment. *J Membr Biol* 188: 151–162.
36. Dvorak MM, et al. (2004) Physiological changes in extracellular calcium concentration directly control osteoblast function in the absence of calciotropic hormones. *Proc Natl Acad Sci USA* 101:5140–5145.
37. Cleemann L, Pizarro G, Morad M (1984) Optical measurements of extracellular calcium depletion during a single heartbeat. *Science* 226:174–177.
38. Pumain R, Heinemann U (1985) Stimulus- and amino acid-induced calcium and potassium changes in rat neocortex. *J Neurophysiol* 53:1–16.
39. Rusakov DA, Fine A (2003) Extracellular Ca^{2+} depletion contributes to fast activity-dependent modulation of synaptic transmission in the brain. *Neuron* 37:287–297.
40. Wiest MC, Eagleman DM, King RD, Montague PR (2000) Dendritic spikes and their influence on extracellular calcium signaling. *J Neurophysiol* 83:1329–1337.
41. Benninger C, Kadis J, Prince DA (1980) Extracellular calcium and potassium changes in hippocampal slices. *Brain Res* 187:165–182.
42. Nicholson C, ten Bruggencate G, Stöckle H, Steinberg R (1978) Calcium and potassium changes in extracellular microenvironment of cat cerebellar cortex. *J Neurophysiol* 41: 1026–1039.
43. Tang L, Hung CP, Schuman EM (1998) A role for the cadherin family of cell adhesion molecules in hippocampal long-term potentiation. *Neuron* 20:1165–1175.
44. Baumgartner W, Golenhofen N, Grundhöfer N, Wiegand J, Drenckhahn D (2003) Ca^{2+} dependency of N-cadherin function probed by laser tweezer and atomic force microscopy. *J Neurosci* 23:11008–11014.
45. Tai CY, Mysore SP, Chiu C, Schuman EM (2007) Activity-regulated N-cadherin endocytosis. *Neuron* 54:771–785.